

Multiple spectator condensates from inflation

Robert J. Hardwick

Institute of Cosmology & Gravitation, University of Portsmouth, Dennis Sciamia Building, Burnaby Road, Portsmouth, PO1 3FX, United Kingdom

E-mail: robert.hardwick@port.ac.uk

Abstract. We investigate the development of spectator (light test) field condensates due to their quantum fluctuations in a de Sitter inflationary background, making use of the stochastic formalism to describe the system. In this context, a condensate refers to the typical field value found after a coarse-graining using the Hubble scale H , which can be essential to seed the initial conditions required by various post-inflationary processes. We study models with multiple coupled spectators and for the first time we demonstrate that new forms of stationary solution exist (distinct from the standard exponential form) when the potential is asymmetric. Furthermore, we find a critical value for the inter-field coupling as a function of the number of fields above which the formation of stationary condensates collapses to H . Considering some simple two-field example potentials, we are also able to derive a lower limit on the coupling, below which the fluctuations are effectively decoupled, and the standard stationary variance formulae for each field separately can be trusted. These results are all numerically verified by a new publicly available python class (`nfield`) to solve the coupled Langevin equations over a large number of fields, realisations and timescales. Further applications of this new tool are also discussed.

Keywords: physics of the early universe, inflation

Contents

1	Introduction	1
2	Vanishing probability current with symmetric potentials	3
3	Computation and analytic arguments	4
3.1	The critical coupling	6
3.2	The decoupling limit	8
3.3	Non-vanishing probability currents	10
4	Conclusions	11
A	Numerical implementation	15

1 Introduction

An effectively massless (light), energetically sub-dominant (test) scalar field placed in an inflationary background is one of the simplest models in which one investigates Quantum Field Theory (QFT) in curved spacetime. Reflecting this simplicity, light test fields — often termed ‘spectator’ fields — have been studied with great detail in the literature [1–9].

As a consequence of these quantum effects, spectator fields typically form condensates during inflation, where here a ‘condensate’ refers to the root mean squared of the distribution over field values in each Hubble patch which one can take to be the typical field value. Such condensates can be used to set the initial conditions for subsequent epochs, e.g., reheating, which connects the inflationary sector to the Standard Model (SM). These initial conditions can therefore depend on the potentials of both the spectator and the inflaton, and hence it is quite natural to consider valid extensions to the standard cases considered in the literature for distinct post-inflationary predictions.

In the same vein, consider now the evolution of multiple spectator fields in the inflationary background. Fields of this type are known to exhibit logarithmic divergences in their correlation functions during inflation, which arise from the accumulation of super-horizon modes sourced by quantum fluctuations that cross the horizon. Due to the unique quantum state [10–12] of such modes during any slow-roll phase, a coarse-graining can be performed over the field at a given physical scale¹. This coarse-graining reveals an Infra-Red (IR) behaviour where the non-commutative components of the field become relatively small when compared with their anti-commuting components. The quantum correction to the classical field dynamics can thus be well-described as a stochastic system of drift and diffusion [15] captured by the following Langevin equation for an indexed field σ_i appearing in a multi-field potential V

$$\frac{d\sigma_i}{dN} = -\frac{1}{3H^2} \frac{\partial V}{\partial \sigma_i} + \frac{H}{2\pi} \xi_i(N), \quad (1.1)$$

¹The coarse-graining scale is typically a Fourier mode $k_{cg} = \epsilon aH$, where ϵ is a parameter which in principle can be linked to the renormalisation scale of the field [13]. In the small ϵ limit, the results from stochastic inflation become independent of ϵ [14].

where ξ_i is a Gaussian white noise term (without cross-correlation) with a unit amplitude ensemble-average $\langle \xi_i(N)\xi_j(N') \rangle = \delta_{ij}\delta(N - N')$ and the dimensionless time variable is the number of e -folds $N \equiv \ln a$ (a being the scale factor). In all equations throughout this paper, we will use the indices $i, j, k = \{1, 2, \dots, n_f\}$, where n_f is the number of spectator fields.

We note here that the correlator form of the noise term in Eq. (1.1) originates from the effectively massless and uncoupled mode functions derived from the vacuum solutions to the field in a quasi-de Sitter background. Should the effective mass $\partial^2 V / \partial \sigma_i^2$ of the field σ_i exceed the Hubble rate, then this formalism is no longer valid and other methods must be developed [16–18]. Hence, it seems natural here to consider the evolution of light fields up until the threshold where their effective mass is equal to the Hubble rate, and beyond which we shall refer to the condensate as having ‘collapsed’ to the Hubble scale and the effective mass has also saturated to H . We shall return to this point in Sec. 3 where we, e.g. evaluate the critical couplings required to achieve this saturation.

For interacting fields in de Sitter spacetimes, another critical value is known to exist which signals the breakdown of the semi-classical approximation. In the mean-field approximation, one separates a classical ‘mean’ background field from perturbatively small quantum fluctuations. For quartic scalar fields, in Ref. [19], it was shown that a breakdown in this perturbative expansion occurs in the regime where the bare mass is less than $\lambda H^2 / (4\pi^2)$ which cannot be removed by reorganising the perturbative expansion to include a running effective mass. We stress here that non-perturbative methods of resummation, such as those of this paper, are potentially unaffected by such a bound. This is due to the fact that the backreaction from small quantum fluctuations is inherently included into the background evolution described by Eq. (1.1), thus optimising the perturbative expansion at each new scale in time — a cosmological analog to (but not exactly the same as [20]) the Renormalisation Group flow [15].

Eq. (1.1) faithfully reproduces the known resummed logarithmic divergences from QFT to leading order [15, 21]. This is usually referred to as the formalism of Stochastic Inflation [22, 23] — which we shall henceforth refer to as the ‘stochastic formalism’. The corresponding Fokker-Planck equation to Eq. (1.1) is

$$\frac{\partial}{\partial N} P(\sigma_i, N) = \frac{1}{3H^2} \sum_{j=1}^{n_f} \frac{\partial}{\partial \sigma_j} \left[\frac{\partial V}{\partial \sigma_j} P(\sigma_i, N) \right] + \frac{H^2}{8\pi^2} \sum_{j=1}^{n_f} \frac{\partial^2}{\partial \sigma_j^2} P(\sigma_i, N), \quad (1.2)$$

where we have implicitly made use of the test field condition $\partial H / \partial \sigma_i = 0$ and defined $P(\sigma_i, N)$ as the probability distribution function over field values at a given N , when normalised. Thus, the evolution of modes as they accumulate outside of the horizon typically yields an n_f -dimensional distribution of field displacements throughout the inflationary phase $P(\sigma_i, N)$.

Eq. (1.2) may also be written essentially as a continuity equation [24, 25]

$$\frac{\partial P}{\partial N} + \sum_{i=1}^{n_f} \frac{\partial J_i}{\partial \sigma_i} = 0, \quad (1.3)$$

where J_i is the probability current and the right hand side of the equation must vanish for probability conservation. By inspection of Eq. (1.2), one may verify that in this case

$$J_i = -\frac{1}{3H^2} \frac{\partial V}{\partial \sigma_i} P(\sigma_i, N) - \frac{H^2}{8\pi^2} \frac{\partial}{\partial \sigma_i} P(\sigma_i, N). \quad (1.4)$$

In de Sitter-like inflation the Hubble parameter is effectively constant in time, hence there is a stationary² solution to Eq. (1.2), P_{stat} , corresponding to a vanishing divergence $\nabla \cdot \mathbf{J} = 0$ of the probability current — an incompressible flow of the vector field with components J_i . Where $n_f = 1$ in an unbounded field domain³ one can show that in order for the distribution to have a finite normalisation $P(\sigma_1, N)d\sigma_1 \rightarrow 0$ (and hence $J_1 \rightarrow 0$) as $\sigma_1 \rightarrow \infty$. Furthermore, given $n_f = 1$, one can also show that in the stationary limit, the vanishing divergence of J_1 simply reduces to $\partial J_1/\partial \sigma_1 = 0$, and J_1 must therefore vanish $\forall \sigma_1$. Hence, the left hand side of Eq. (1.4) may always be set to zero and the well-known exponential solution to Eq. (1.2) for the stationary probability distribution is obtained [23] $P_{\text{stat}}(\sigma_1) \propto \exp[-8\pi^2 V(\sigma_1)/3H^4]$.

For unbounded V with arbitrary n_f , it is still natural to consider a boundary condition where $J_i = 0$ as $\sigma_i \rightarrow \infty$ to restrict unphysical possibilities, and this may even in practice occur at a set finite scale Λ that denotes the chosen cutoff of the theory. However, one can no longer generally state that J_i vanishes everywhere throughout the n_f -field domain since any class of incompressible vector J_i flows are permitted. Because $\partial J_i/\partial \sigma_i = 0$ is still possible, it is true that one stationary solution to Eq. (1.2) is

$$P_{\text{stat}}(\sigma_i) \propto \exp\left[-\frac{8\pi^2 V(\sigma_i)}{3H^4}\right], \quad (1.5)$$

but it is no longer unique, and one must use either use further analytical arguments or full numerical solutions for verification.

For any n_f , the stationary distribution P_{stat} is in practice only reached after some equilibration timescale N_{eq} . The timescale N_{eq} is defined as the number of e -folds it takes for $P(\sigma_i, N) = \prod_{i=1}^{n_f} \delta(\sigma_i)$ — an n_f -dimensional Dirac delta function⁴ — to relax to $P(\sigma_i, N) = P_{\text{stat}}$. Hence, N_{eq} can be thought of as the time it takes for the effective condensate to grow to its maximal value in every field dimension. It is also important to note here that the definition of N_{eq} used in this paper relies on the inflationary background being de Sitter-like. In slow-roll backgrounds where H varies more substantially, such as those permitted by a monomial $U(\phi) \propto \phi^p$ inflationary potential, this timescale will have to be recomputed [8].

2 Vanishing probability current with symmetric potentials

In the previous section, we stated that the exponential form (Eq. (1.5)) of the stationary solution to Eq. (1.2) may no longer be stable when any divergence-free (incompressible) probability currents are potentially allowed. For any choice of $n_f > 1$, only the divergence of the current must vanish for a stationary solution, which leaves the possibility of a curl in the vector field $\nabla \times \mathbf{J}$. Because $\mathbf{J} \cdot \hat{\mathbf{e}}$ vanishes, where $\hat{\mathbf{e}}$ is the normal to the boundary, the total integral of the curl over the domain of the fields $\sigma_i \in \Sigma$ vanishes according to Stokes' theorem

$$\int_{\Sigma} (\nabla \times \mathbf{J})_i d^{n_f} \sigma_i = 0, \quad (2.1)$$

² $\partial P/\partial N = 0$ in this context.

³In the case of a bounded field domain, probability conservation at the specified boundary implies that $J_i = 0$ directly.

⁴We note that, for the symmetric potentials about the origin used in this paper, this is of course equivalent to the more general definition of a Dirac function at the global minimum, $\prod_{i=1}^{n_f} \delta(\sigma_i - \sigma_i^{\text{min}})$.

however there are still an infinite number of functions for $\nabla \times \mathbf{J}$ that can satisfy this criterion. Examining Eq. (1.4), and using the general properties of the totally antisymmetric symbol ϵ_{ijk} , one can show that

$$(\nabla \times \mathbf{J})_i = - \sum_{j=1}^{n_f} \sum_{k=1}^{n_f} \epsilon_{ijk} \frac{1}{3H^2} \frac{\partial V}{\partial \sigma_k} \frac{\partial P}{\partial \sigma_j}. \quad (2.2)$$

Our first remark is that Eq. (2.2) vanishes at the extrema of V and P (a fact that we numerically verify for a given potential in Sec. 3.3) but not necessarily everywhere in the domain of σ_i . Secondly, for all choices of potential and initial distribution, if the gradients of V and P align, i.e. $\partial V / \partial \sigma_i \propto \partial P / \partial \sigma_i$, then Eq. (2.2) vanishes and hence $J_i = 0$ must be true at this point. If one takes a derivative of Eq. (1.5), it is clear that the stationary solution that we have quoted satisfies this criterion.

Without an alternative ansatz to compute P , it is difficult to make any general claims about stationary solutions to Eq. (1.2), even when V is symmetric⁵. However, we conjecture that when V is symmetric, the solution for P — which we assume has a been evolved from a symmetric initial condition — typically has a gradient which aligns with V and hence Eq. (1.5) is a stable stationary solution to Eq. (1.2). We have verified numerically that Eq. (1.5) provides a stable solution to the late-time dynamics with symmetric potentials in Sec. 3. Note also that in asymmetric potentials⁶ we can no longer assume that the J_i components vanish everywhere, and Eq. (1.5) is no longer the stationary solution. In such instances, one can also turn to numerical methods.

3 Computation and analytic arguments

The general problem for arbitrary V defined by Eqs. (1.1) and (1.2) cannot be solved analytically, and so in this section we shall make our computations for the condensates formed from multi-field spectator potentials combining both analytic and numerical methods. The details of our numerical implementation can be found in the Appendix A, where we briefly outline our development of a new publicly available python code, `nfield`.

In light of our discussion in Sec. 2, we cannot always expect to use moments of the distribution in Eq. (1.5) to reliably evaluate the stationary variance for asymmetric potentials. However, we shall not need this distribution to hold true in order to still gain an insight from some approximations.

Consider a general multi-field interacting spectator potential. In the limit of small field displacements, one can typically perform a Taylor expansion about the minimum of a

⁵Indeed, even with symmetric V and P (the latter can be proved to follow from a symmetric initial condition), if $n_f = 2$ it can be shown that

$$(\nabla \times \mathbf{J})_3 = f(\sigma_1, \sigma_2) - f(\sigma_2, \sigma_1), \quad (2.3)$$

where $f(\sigma_1, \sigma_2)$ is an arbitrary function of both variables. Eq. (2.3) trivially satisfies the integral constraint from Stokes' theorem (Eq. (2.1)) and hence we are left with no further determination of its exact form without working through an explicit example. Note, however, that Eq. (2.3) gives $(\nabla \times \mathbf{J})_3(\sigma_1, \sigma_2) = -(\nabla \times \mathbf{J})_3(\sigma_2, \sigma_1)$ and hence, if one can also demonstrate that $\mathbf{J}(\sigma_1, \sigma_2) = \mathbf{J}(\sigma_2, \sigma_1)$ for symmetric potentials, it must be true that $(\nabla \times \mathbf{J})_3 = 0$.

⁶For example, some of the potentials we introduce and discuss in Sec. 3.2.

potential which defines an effective mass in each orthogonal field dimension⁷ as

$$M_i^2 \equiv \frac{\partial^2 V}{\partial \sigma_i^2}. \quad (3.1)$$

Hence, a generic multi-field potential can be approximated by

$$V \simeq \frac{1}{2} \sum_{j=1}^{n_f} M_j^2 \sigma_j^2, \quad (3.2)$$

where one may account for interactions (both self and with other fields) through the typical values that one finds for M_i . For example, quartic self-interacting terms where $M_i \propto \sigma_i$ may be approximately written as $M_i \propto \sqrt{\langle \sigma_i^2 \rangle}$. As another example, consider the situation where $M_i \propto \sigma_k^2$ due to interaction terms, then the effective mass becomes approximately $M_i \propto \langle \sigma_k^2 \rangle$. This approximation will prove sufficient to calculate the desired quantities in Sec. 3.1.

Using Eq. (3.2), one can derive a second-moment evolution equation from Eq. (1.1) of the form [1]

$$\frac{d \langle \sigma_i^2 \rangle}{dN} \simeq -\frac{2M_i^2}{3H^2} \langle \sigma_i^2 \rangle + \frac{H^2}{4\pi^2}, \quad (3.3)$$

and hence the stationary⁸ variance can be immediately derived⁹ [1]

$$\langle \sigma_i^2 \rangle |_{\text{stat}} = \frac{3H^4}{8\pi^2 M_i^2}. \quad (3.4)$$

Note that in the limit where Eq. (3.2) is no longer an approximation, such as for a quadratic non-interacting spectator, then Eq. (3.3) and Eq. (3.4) are precise equations with M_i corresponding to the bare mass.

In Eq. (3.4), the inverse-proportionality between the effective mass and the variance indicates that there is a critical value for $M_i \simeq H$ above which the stationary condensate collapses to the Hubble rate $\sqrt{\langle \sigma_i^2 \rangle} = H$. Taking a two-field example for illustration, we have plotted a schematic diagram of the physical situation in Fig. 1 for a symmetric potential. In the left panel, the condensate (dashed black circle) is relatively large because the effective mass $M_i \ll H$. In the right panel, the condensate collapses to the value of the Hubble rate (dashed red circle) because $M_i \simeq H$. For the shaded red region the suppression $\langle \sigma_i^2 \rangle \propto 1/M_i^2$ in the variance from Eq. (3.4) is no longer valid and the stochastic approach can no longer be used. This is because when $M_i > H$ the mode functions which source the fluctuations of the field can no longer be accurately described by the simple form of noise correlator in the definition of Eq. (1.1).

Other calculations do exist for situations considering a constant super-Hubble mass $M_i > H$ [16–18] where, in these instances, the variance is known to experience further suppression. However, the assumption of constant M_i is one we cannot make for the potentials studied in this work. We anticipate that a similar suppression occurs but leave the verification

⁷Where we have already implicitly performed any necessary rotations in field space such that $\sigma_i \sigma_j$ cross-terms vanish.

⁸ $d \langle \sigma_i^2 \rangle / dN = 0$ in this context, hence this need only be ‘stationary’ in the i th field dimension.

⁹Notice that this equation is indeed consistent with inserting Eq. (3.2) into Eq. (1.5) and taking the second-order moment.

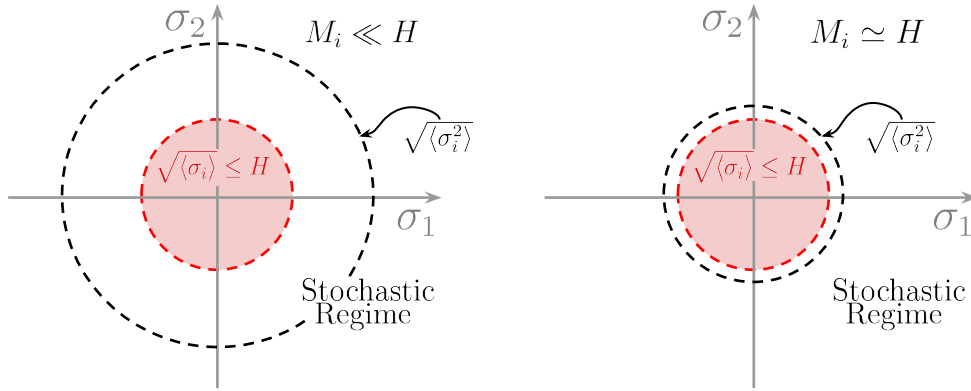


Figure 1. Schematic diagrams of the condensate $\sqrt{\langle \sigma_i^2 \rangle}$ (dashed black circles) in a symmetric two-field potential. When $M_i \simeq H$ the condensate collapses to the Hubble rate, corresponding to the dashed red circle. The shaded red region corresponds to situations where $M_i > H$ and there is conjectured saturation at the Hubble scale $\sqrt{\langle \sigma_i^2 \rangle} \simeq H$. The entire region in field space outside of the red shaded area can be considered where the stochastic formalism is valid, with the caveat that it is possible for $M_i > H$ to also occur for a field at large displacements, e.g. quartic self-interacting fields will have $M_i \propto \sigma_i$.

of this to future work. Even if this is not always true (e.g. for many non-interacting quadratic spectators), the ‘saturation’ value is still of interest since it characterises the fundamental domain of validity for the stochastic formalism. Hence, in this regard, we shall leave the calculation of possible condensates in the $M_i > H$ regime to future work, and therefore we will work within the regime where the stochastic formalism is valid.

3.1 The critical coupling

In this subsection, we will demonstrate that when one generalises the formation of spectator field condensates to many coupled fields, a critical value for the coupling appears, above which the equilibrium variances of all fields have collapsed to the Hubble scale and effective mass of each field has saturated to H . To show this we will consider a simplified potential that will allow us to calculate this critical coupling both analytically and numerically, for verification.

Now consider the multi-field spectator potential

$$V_A = \frac{1}{2}g \sum_{i \neq j} \sigma_i^2 \sigma_j^2. \quad (3.5)$$

Mindful of the approximation made with M_i in Eq. (3.2), one thus expects that incrementally strengthening the interaction between spectator fields $\propto g\sigma_i^2\sigma_j^2$ can lead to the eventual saturation of the condensate value at the Hubble scale due to the effective mass of each field being progressively larger, and we therefore anticipate a critical value for the inter-field coupling g_{crit} to exist, for a given n_f , above which the stationary condensate collapses to $\sqrt{\langle \sigma_i^2 \rangle} \simeq H$.

By inspection between Eqs. (3.2) and (3.5), the typical value of the effective mass in the i th field dimension corresponds to $M_i^2 \simeq g \sum_{k \neq i} \langle \sigma_k^2 \rangle \simeq g(n_f - 1) \langle \sigma_i^2 \rangle$, where in the

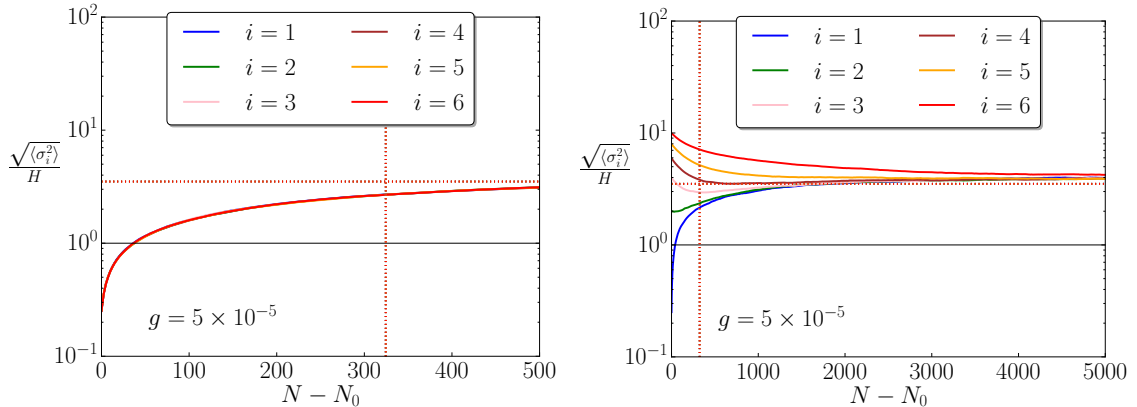


Figure 2. The numerically evaluated (solid lines) time evolution of the variance for each spectator field in the case of the V_A potential (Eq. (3.5)) with example value $n_f = 6$. The variance of all fields is initialised at $\langle \sigma_i^2 \rangle = 0$ in the left panel and we have chosen a range of initial conditions for the fields in the right panel to indicate the robustness of the late time stationary behaviour. All of the field variances overlap due to the symmetry of the potential. Dotted horizontal and vertical lines represent the stationary variance (Eq. (3.6)) and equilibration timescale (Eq. (3.8)), respectively. The number of realisations used is 10^4 .

second equality we have assumed that the distribution (using Eq. (3.5) as the potential) has reached stationarity $P(\sigma_i, N) = P_{\text{stat}}$ and, hence, due to symmetry $\langle \sigma_i^2 \rangle = \langle \sigma_k^2 \rangle \forall i, k$. Because $\langle \sigma_i^2 \rangle = \langle \sigma_i^2 \rangle|_{\text{stat}}$, given in Eq. (3.4), we can now obtain an approximate relation for the critical coupling¹⁰

$$\begin{aligned} \langle \sigma_i^2 \rangle &= \frac{3H^4}{8\pi^2 M_i^2} \simeq \frac{3H^4}{8\pi^2 g(n_f - 1) \langle \sigma_i^2 \rangle} \\ \Rightarrow \langle \sigma_i^2 \rangle &\simeq \sqrt{\frac{3H^4}{8\pi^2 g(n_f - 1)}} \end{aligned} \quad (3.6)$$

$$\Rightarrow g_{\text{crit}} \simeq \frac{3}{8\pi^2(n_f - 1)}, \quad (3.7)$$

where we have found g_{crit} by setting $\langle \sigma_i^2 \rangle = H^2$ in Eq. (3.6).

For illustration, we plot the time evolution for variances, averaging over multiple Langevin realisations (realisations of Eq. (1.1)), of an example where $n_f = 6$ in Fig. 2 and Eq. (3.6) is shown to be a good description of the stationary values against the numerically evaluated variances (all identical to each other due to the symmetry). The approximate form of Eq. (3.7) must also be verified numerically, and hence we plot in Fig. 3 the comparison between numerical and analytic approaches to obtain the functional relationship between $g_{\text{crit}}(n_f)$. Due to the apparently excellent agreement between the two calculations in Fig. 3 we can be confident in Eq. (3.7) as a reliable formula to extrapolate to large n_f .

We further note that one may derive the equilibration timescale for each field dimension

¹⁰Note that because Eq. (3.5) is a symmetric potential — i.e. $V(\sigma_j) = V(\sigma_{\text{perm}(j)})$ for any permutation of field indices $\text{perm}(j)$ — our discussion in Sec. 2 indicates the stability of Eq. (1.5) in this situation. Hence, another way to compute Eq. (3.6) would be to take the second moment of Eq. (1.5).

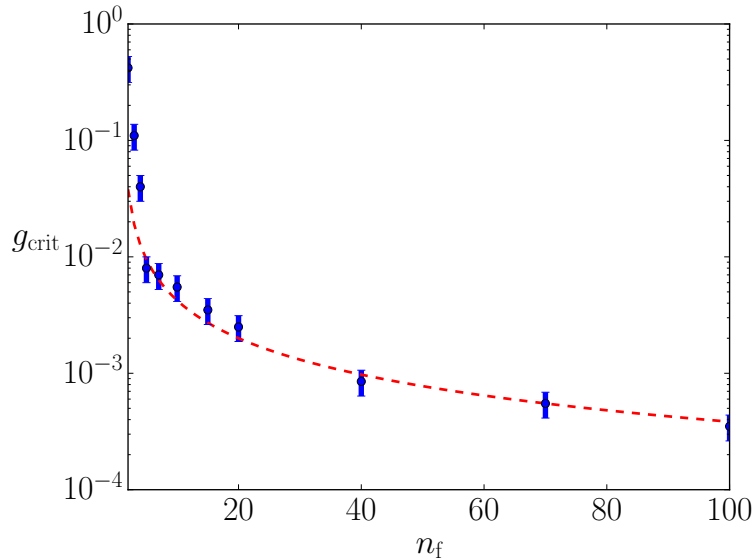


Figure 3. The numerically evaluated (blue data points with error bars related to both statistical and numerical uncertainty from having a finite number of realisations and a finite stepsize in numerically finding g_{crit} , respectively) value of g_{crit} as a function of the number of fields n_f for potential V_A (see Eq. (3.5)). The line clearly matches the analytically derived relation in Eq. (3.7) (dashed red line) very well. The number of realisations used is 10^4 for each point. Due to how rapidly g_{crit} varies with the number of fields for $n_f \lesssim 5$, we are likely underestimating our error in this region, and hence these points may appear slightly inconsistent.

$N_{\text{eq},i}$ for the V_A potential, and this is approximately be given by

$$N_{\text{eq},i} \simeq \frac{H^2}{M_i^2} \simeq \sqrt{\frac{8\pi^2}{3g(n_f - 1)}}. \quad (3.8)$$

The first relation of Eq. (3.8) can be derived from Eq. (3.3) (see also Refs. [7, 8, 23]), where it is also natural to consider the ‘steepness’ of the effective potential in Eq. (3.2) to control the rate of equilibration. Note that Eq. (3.8) has been derived by assuming the stationary variance, however, because $N_{\text{eq},i}$ is precisely the time it takes to relax to the stationary limit, this assumption is not strictly valid and requires comparison with full numerical solutions. Interestingly, in the example with $n_f = 6$ plotted in Fig. 2, Eq. (3.8) appears to perform well regardless of its less trustworthy origin.

3.2 The decoupling limit

We will now investigate another limit of the inter-field coupling, which can also be analytically estimated for some specific potentials and the numerical verification will also serve to showcase further applications of the `nfield` code.

Consider two further examples of interacting spectator potentials

$$V_B = \frac{1}{2}m^2(\sigma_1^2 + \alpha\sigma_2^2) + \frac{1}{2}g\sigma_1^2\sigma_2^2 \quad (3.9)$$

$$V_C = \frac{1}{4}\lambda(\sigma_1^4 + \alpha\sigma_2^4) + \frac{1}{2}g\sigma_1^2\sigma_2^2. \quad (3.10)$$

V_B a generalisation from V_A by introducing additional masses m and $\sqrt{\alpha}m$, with a hierarchy parameter α , but we have now specified that $n_f = 2$ to capture the essential phenomenology. V_C is another generalisation from V_A to include self-interactions. We note here that, in each case, decoupling the system in the limit where $g \rightarrow 0$ will yield the well-known formulae [7, 8, 23] for the stationary variance of each non-interacting field (see Eq. (3.4))

$$\text{Decoupled } V_B \Rightarrow \langle \sigma_1^2 \rangle |_{\text{stat}} = \frac{3H^4}{8\pi^2 m^2} \quad (3.11)$$

$$\langle \sigma_2^2 \rangle |_{\text{stat}} = \frac{3H^4}{8\pi^2 \alpha m^2} \quad (3.12)$$

$$\text{Decoupled } V_C \Rightarrow \langle \sigma_1^2 \rangle |_{\text{stat}} = \frac{\Gamma(\frac{3}{4})}{\Gamma(\frac{1}{4})} \sqrt{\frac{3H^4}{2\pi^2 \lambda}} \quad (3.13)$$

$$\langle \sigma_2^2 \rangle |_{\text{stat}} = \frac{\Gamma(\frac{3}{4})}{\Gamma(\frac{1}{4})} \sqrt{\frac{3H^4}{2\pi^2 \alpha \lambda}}. \quad (3.14)$$

In this same limit one can also obtain the respective equilibration timescales

$$\text{Decoupled } V_B \Rightarrow N_{\text{eq},1} |_{\text{stat}} \simeq \frac{H^2}{M_1^2} \simeq \frac{H^2}{m^2} \quad (3.15)$$

$$N_{\text{eq},2} |_{\text{stat}} \simeq \frac{H^2}{M_2^2} \simeq \frac{H^2}{\alpha m^2} \quad (3.16)$$

$$\text{Decoupled } V_C \Rightarrow N_{\text{eq},1} |_{\text{stat}} \simeq \frac{H^2}{M_1^2} \propto \frac{1}{\sqrt{\lambda}} \quad (3.17)$$

$$N_{\text{eq},2} |_{\text{stat}} \simeq \frac{H^2}{M_2^2} \propto \frac{1}{\sqrt{\alpha \lambda}}, \quad (3.18)$$

where we recall that the effective masses M_i are defined in Eq. (3.1). We note there that, as in Eq. (3.8), these timescales have been derived using the stationary form of the variances which is not strictly valid, hence they must be checked for validity against the numerical implementation to ensure that they are still accurate.

A ‘decoupling’ value of $g = g_{\text{dec}}$ can be derived analytically from these stationary variances by obtaining the value of g above which the main contribution to the effective mass is from the coupling term $\propto g$ and not from the bare mass or self-interaction. Looking at the effective mass of either of the fields in each potential, one can hence show that in the stationary limit

$$V_B \Rightarrow M_1^2 \simeq m^2 + g \langle \sigma_2^2 \rangle |_{\text{stat}} \Rightarrow g_{\text{dec}} \simeq \frac{8\pi^2}{3} \alpha \left(\frac{m}{H} \right)^4 \quad (3.19)$$

$$V_C \Rightarrow M_1^2 \simeq 3\lambda \langle \sigma_1^2 \rangle |_{\text{stat}} + g \langle \sigma_2^2 \rangle |_{\text{stat}} \Rightarrow g_{\text{dec}} \simeq 3\lambda \sqrt{\alpha}. \quad (3.20)$$

If one were to re-derive Eq. (3.19) and Eq. (3.20) by replacing $M_1 \iff M_2$, it is trivial to show that the same formulae are obtained.

If $g > g_{\text{dec}}$ and $\alpha \neq 1$ however, then neither the equations above, nor the symmetry of $P(\sigma_i, N)$, can be exploited for analytic calculations and hence one must rely upon the numerically evaluated solution in order to study the system. In Fig. 4 and Fig. 6 we plot these numerical solutions (and their corresponding effective masses in Fig. 7 and Fig. 8) given some specific values of $(m \text{ or } \lambda, \alpha, g)$ for both fields in the quadratic and quartic potentials,

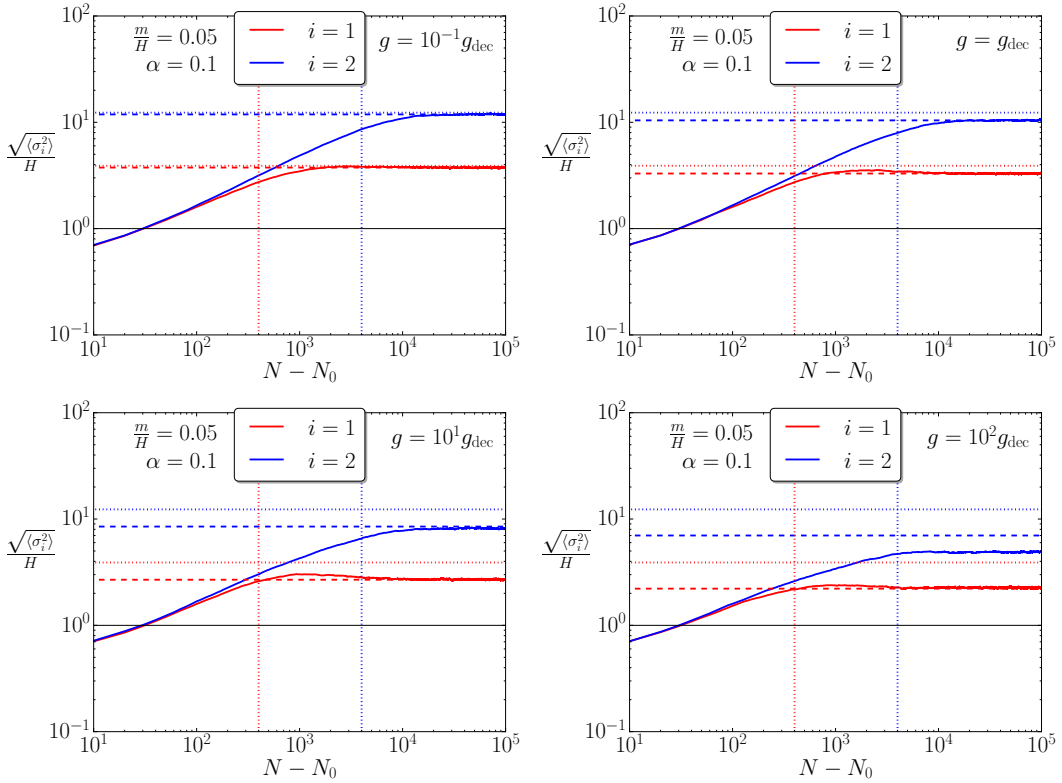


Figure 4. The numerically evaluated (solid lines) time evolution of the variance for each spectator field in the case of the V_B potential (see Eq. (3.9)), where variance of both fields is initialised at $\langle \sigma_i^2 \rangle = 0$ and 10^4 realisations of Eq. (1.1) were used in `nfield`. Dotted horizontal and dotted vertical lines represent the stationary variances (Eqs. (3.11) and (3.12)) and equilibration timescales (Eqs. (3.15) and (3.16)), respectively, computed in the decoupled limit $g \leq g_{\text{dec}}$. The dashed horizontal lines use an alternative method to derive the stationary variance by numerically evaluating the second moment of Eq. (1.5). The number of realisations used in each case is 10^4 .

respectively. The variances are all initialised with $\langle \sigma_i^2 \rangle = 0$ and hence the number of e -folds it takes for each solution to reach the effectively decoupled stationary values (dotted horizontal lines in the relevant colour using Eqs. (3.11), (3.12), (3.13) and (3.14)) is well-approximated by the analytic relaxation timescales derived in Eqs. (3.15), (3.16), (3.17) and (3.18) (depicted with vertical dotted lines in the relevant colour) in cases where $g \leq g_{\text{dec}}$ (the top row plots of both sets of Figs.). In all plots, one can also clearly see the strong deviation from the decoupled predictions with larger values of g , which highlights the importance for a numerical solution from `nfield` in this large regime of parameter values to obtain the correct equilibrium as well as out-of-equilibrium behaviour.

3.3 Non-vanishing probability currents

In Fig. 4 there is also an important anomaly which appears to be repeated in Fig. 6. In both figures we have also provided (dashed horizontal lines) an alternative calculation for the stationary variance using the numerically calculated second moment of Eq. (1.5). There is generally excellent agreement between this solution and the one obtained from the many realisations of Eq. (1.1) in `nfield` for $g \leq 10g_{\text{dec}}$, however these no longer agree precisely

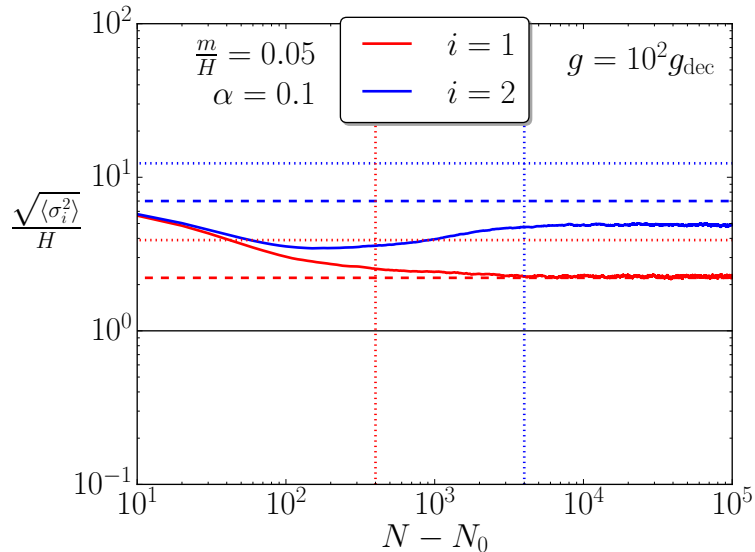


Figure 5. An illustrative re-plotting of the numerical variance evolution, with an initial condition much closer to the analytic stationary variance derived from the second moment of Eq. (1.5), for the case in the bottom right-hand corner of Fig. 4.

when $g = 10^2 g_{\text{dec}}$ in both sets of plots. This deviation has been checked for numerical robustness by increasing the number of Langevin realisations to 10^5 and altering the initial conditions — see Fig. 5 for illustration.

We are left with the interesting conclusion that for a sufficiently large coupling g , and an asymmetric potential induced by the mass hierarchy parameter $\alpha < 1$, Eq. (1.5) is no longer sufficient to describe the stationary probability distribution. In Sec. 2 we conjectured that Eq. (1.5) is the stationary solution for symmetric potentials (here when $\alpha = 1$). However, when $\alpha < 1$, since only the divergence of the probability current $\nabla \cdot \mathbf{J}$ must vanish and *not* its curl $\nabla \times \mathbf{J}$, Eq. (1.5) is no longer the true stationary solution and hence the solution must be elucidated through full numerical evaluation of either Eq. (1.1) or Eq. (1.2). We have plotted $\nabla \times \mathbf{J}$ for different choices of parameter in Fig. 9 and Fig. 10, where one can see in particular that the only component of $\nabla \times \mathbf{J}$ is much larger when g is increased for the $\alpha = 0.1$ cases plotted in Fig. 10. As a further numerical check, we have verified that when the symmetry of the potential is restored ($\alpha = 1$) in Fig. 9, the curl vanishes up to some numerical noise.

Note that $\nabla \times \mathbf{J}$ also vanishes at the origin in both Fig. 9 and Fig. 10. This is confirmed by the analytic expression in Eq. (2.2), in which the curl is indeed vanishing at the extrema $\partial V / \partial \sigma_i = \partial P / \partial \sigma_i = 0$.

4 Conclusions

In this paper we have demonstrated the usefulness of numerical solutions in order to evaluate the variances of multiple light coupled fields during inflation. In doing so we have identified a lower limit g_{dec} in some example two-field potentials on the coupling g , for interactions of the form $\propto g \sigma_1^2 \sigma_2^2$, below which the fields may be considered as effectively decoupled and the standard formulae for stationary variances may be used. We have further verified

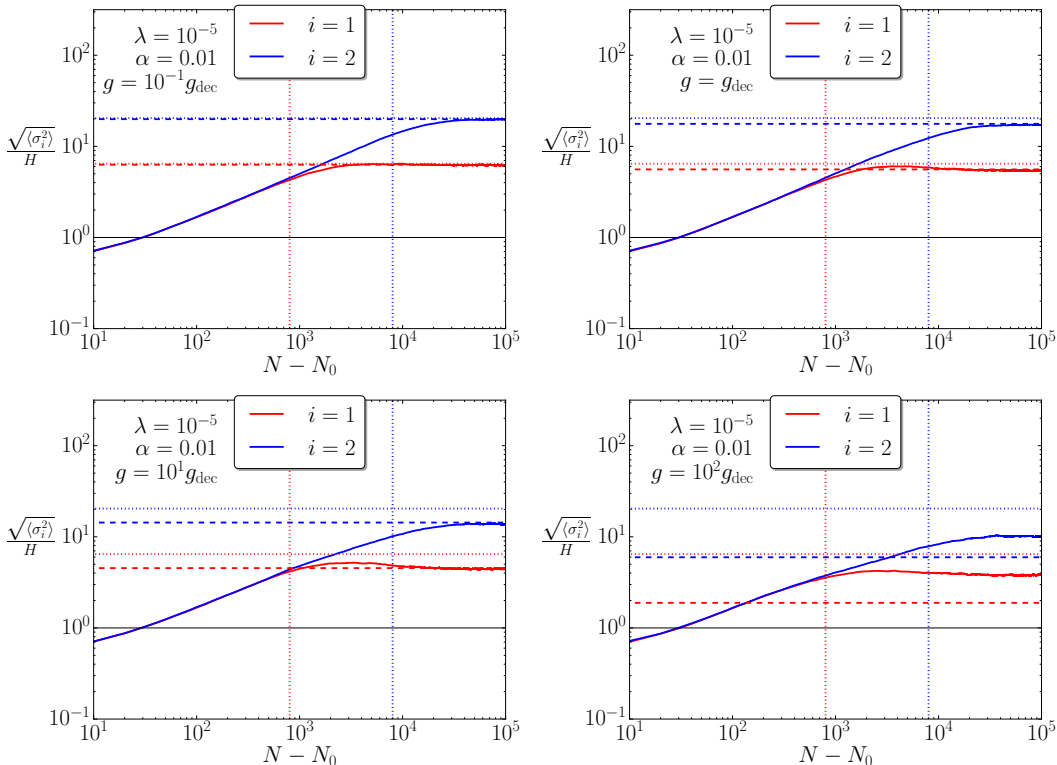


Figure 6. The numerically evaluated (solid lines) time evolution of the variance for each spectator field in the case of the V_C potential (see Eq. (3.10)), where variance of both fields is initialised at $\langle \sigma_i^2 \rangle = 0$ and 10^4 realisations of Eq. (1.1) were used in `nfield`. Dotted horizontal and dotted vertical lines represent the stationary variances (Eqs. (3.13) and (3.14)) and equilibration timescales (Eqs. (3.17) and (3.18)), respectively, computed in the decoupled limit $g \leq g_{\text{dec}}$. The dashed horizontal lines use an alternative method to derive the stationary variance by numerically evaluating the second moment of Eq. (1.5). The number of realisations used in each case is 10^4 .

that for choices of $g \geq g_{\text{dec}}$, the analytic decoupling approximation for the variances breaks down. In such situations, the solutions from either evaluating the moments of Eq. (1.5) (Eqs. (3.9) and (3.10), stable in the stationary limit when the potential is either symmetric $\alpha = 1$ or decoupled $g < g_{\text{dec}}$) or full numerical solutions (for all potentials and generic initial conditions) are the methods to obtain correct values.

In Sec. 2 we have given a general argument as to why it is possible for Eq. (1.5) to still remain stable for some symmetric potentials due to vanishing of the probability current everywhere in the domain. Conversely, we have shown that by breaking the symmetry in the potential (e.g. $\alpha \neq 1$ in Eqs. (3.9) and (3.10)) the form of Eq. (1.5) may no longer be stable as a solution to the stationary behaviour of the multi-spectator system. We have supported these conclusions with the numerically obtained figures provided in Sec. 3.2 and Figs. 9 and 10.

A simple generalisation for future work may be to check how this limit changes as the number of coupled fields n_f is increased, where we anticipate that because increasing n_f typically increases the contribution from the coupling to the effective mass of each field, the lower limit on $g = g_{\text{dec}}$ should decrease in order to compensate. Due to the complexity of such

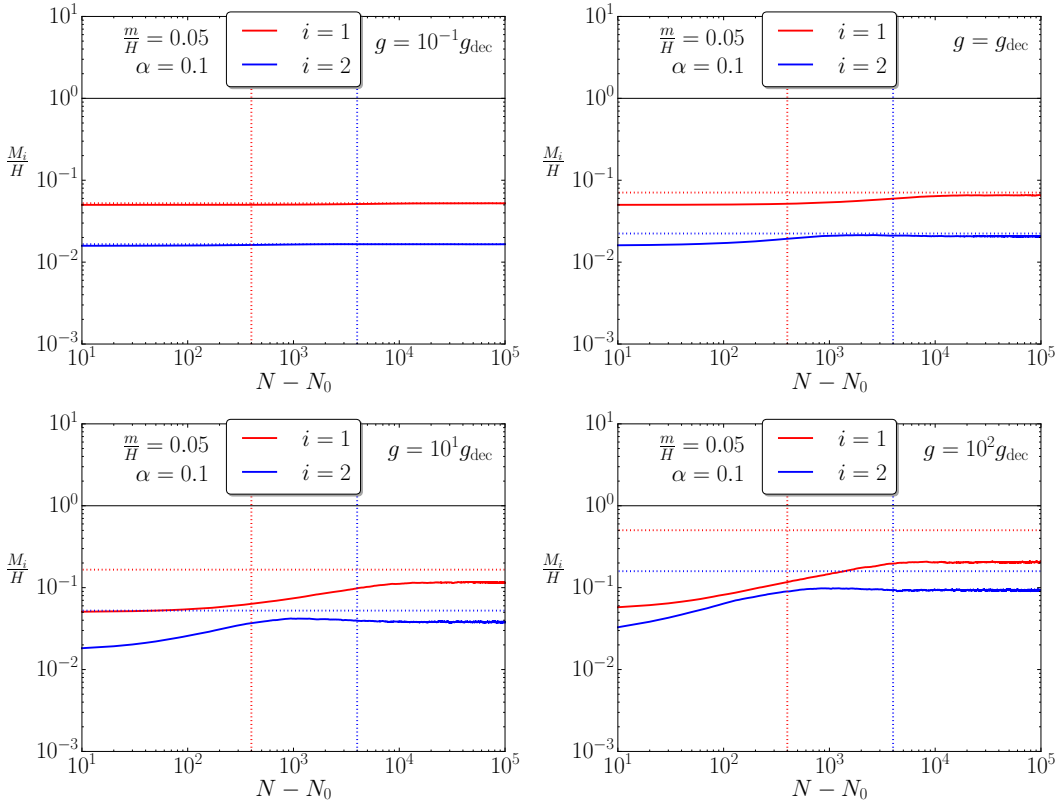


Figure 7. The numerically evaluated (solid lines) time evolution of the effective mass (see Eq. (3.1)) for each spectator field in Fig. 4. Dotted horizontal and dotted vertical lines represent M_i derived using the stationary variances (Eqs. (3.11) and (3.12)) and the equilibration timescales (Eqs. (3.15) and (3.16)), respectively.

a system, a numerical scheme such as the one we have developed in this paper¹¹ (`nfield`) will likely be required for such an extension.

By considering an arbitrary n_f in the symmetric potential of Eq. (3.5) we have also discovered a critical value for $g = g_{\text{crit}}$ that varies $\propto 1/n_f$ (see Eq. (3.7) for a more precise form) above which the formation of stationary spectator condensates collapses to the Hubble rate. For values of $g > g_{\text{crit}}$, we cannot yet precisely say that the formation of stationary condensates in such a potential is suppressed (as it is when increasing g up to this point) because this phenomenon results from the effective mass M_i of each field reaching $\mathcal{O}(1)H$. At this point the mode functions which source the fluctuations of the field can no longer be accurately described by the simple form of noise correlator in the definition of Eq. (1.1), and hence the stochastic formalism cannot be exactly trusted when $M_i > H$. It is known [16–18], however, that the suppression may be further enhanced when $M_i > H$ — assuming that M_i is constant — and so we anticipate that further (perhaps fully QFT-theoretic) computations to include a field-dependent effective mass in future work may support our current conjecture beyond this point.

In extended work it would be interesting to study the effect of a number of alternative

¹¹One can go to the following repository to access the code: <https://github.com/umbralcalc/nfield>.

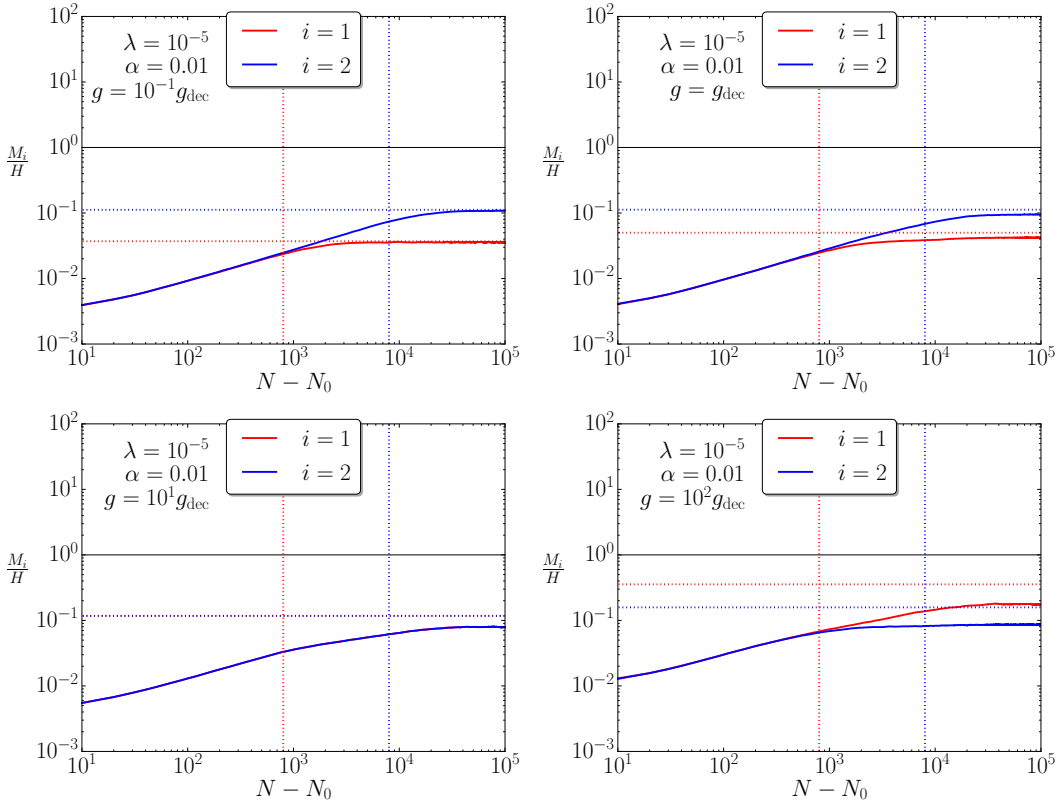


Figure 8. The numerically evaluated (solid lines) time evolution of the effective mass (see Eq. (3.1)) for each spectator field in Fig. 6. Dotted horizontal and dotted vertical lines represent M_i derived using the stationary variances (Eqs. (3.13) and (3.14)) and the equilibration timescales (Eqs. (3.17) and (3.18)), respectively.

couplings on the formation of post-inflationary spectator condensates, such as e.g. trilinear couplings (as in the case of the Higgs [26]) and couplings of multiple fields to the inflationary sector (as in ‘M-flation’ [27] or the newly proposed model of ‘Horizon Feedback Inflation’ [28]). The abundance of post-inflationary condensates can also be known to affect various models of dark energy [29], dark matter [30], and the reheating decay efficiency of the inflaton through Higgs thermal blocking [31]. Even from these few examples, it is clear that precise numerical predictions provide an important component in providing the initial conditions to model building in the early Universe.

Acknowledgements

The author is supported by UK Science and Technology Facilities Council grant ST/N5044245. Some numerical computations were done on the Sciama High Performance Compute (HPC) cluster which is supported by the ICG, SEPNet and the University of Portsmouth. The author would also like to thank both Matthew Hull for fruitful discussions and Chris Pattison, Vincent Vennin and David Wands for careful reading and helpful comments on the manuscript.

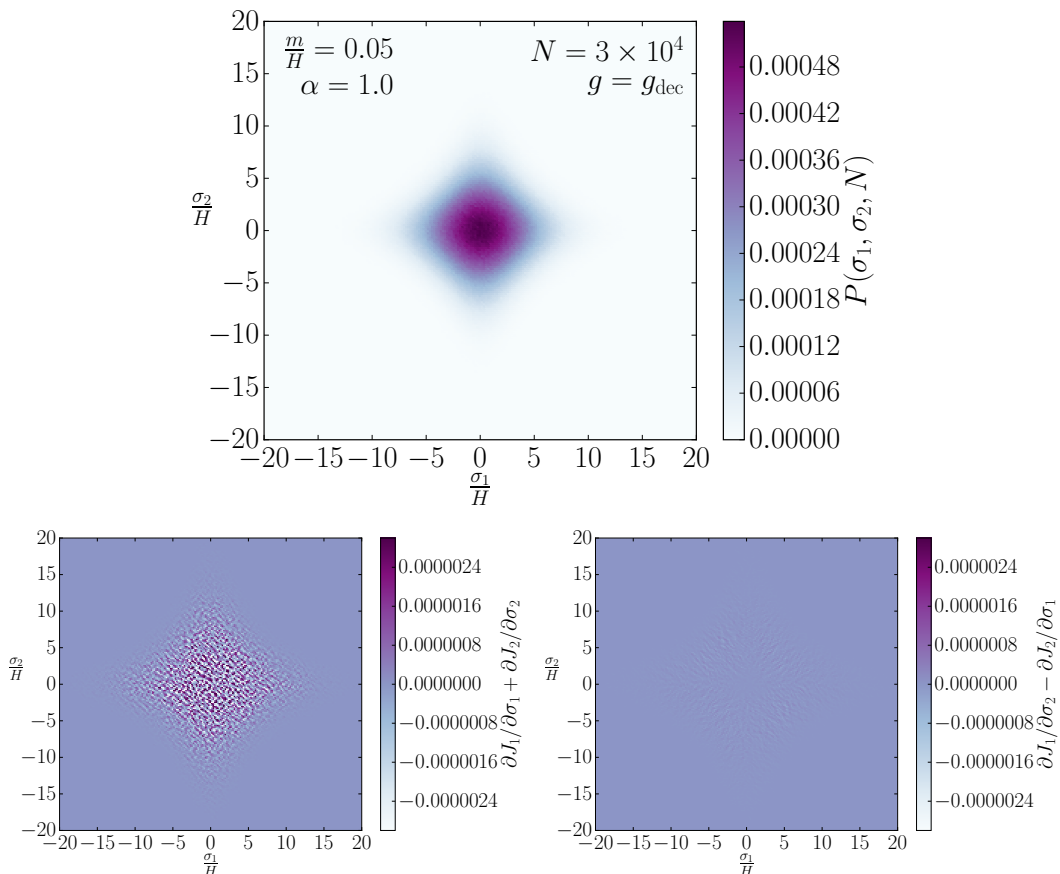


Figure 9. Using specific parameter choices of the V_B potential (see Eq. (3.9)) we plot the binned stationary probability density P_{stat} (on top), probability current divergence $\nabla \cdot \mathbf{J}$ (bottom left) and the only non-zero component of the probability current curl $\nabla \times \mathbf{J}$ (bottom right). These have all been numerically obtained from 10^7 realisations of Eq. (1.1) in the `nfield` code.

A Numerical implementation

Few analytic solutions to either Eq. (1.1) or Eq. (1.2) for $n_f \geq 2$ are known to exist, except in the stationary limit of various cases, as given in Eq. (1.5). A robust method for numerical evaluation of a coupled system of Langevin equations of the form in Eq. (1.1) is the modified Improved Euler scheme, introduced in Ref. [32], where it is also proven to exhibit strong first-order convergence. Due to the more complicated potentials studied, a relatively simple implementation of this scheme was developed for the numerical solutions obtained in this work.

The code is written in the python language and achieves runtimes of ~ 5 -10 minutes on a standard netbook laptop for 10^4 realisations of with any potential up to $n_f \sim 10$ for 10^5 e -folds. For increased performance, e.g. $n_f \sim \mathcal{O}(100)$ or more, then it is advised to use a computer cluster. The code has also been made publicly available at the following repository: <https://github.com/umbralcalc/nfield>. The repository also contains an example script with 5 fields to help the user get started.

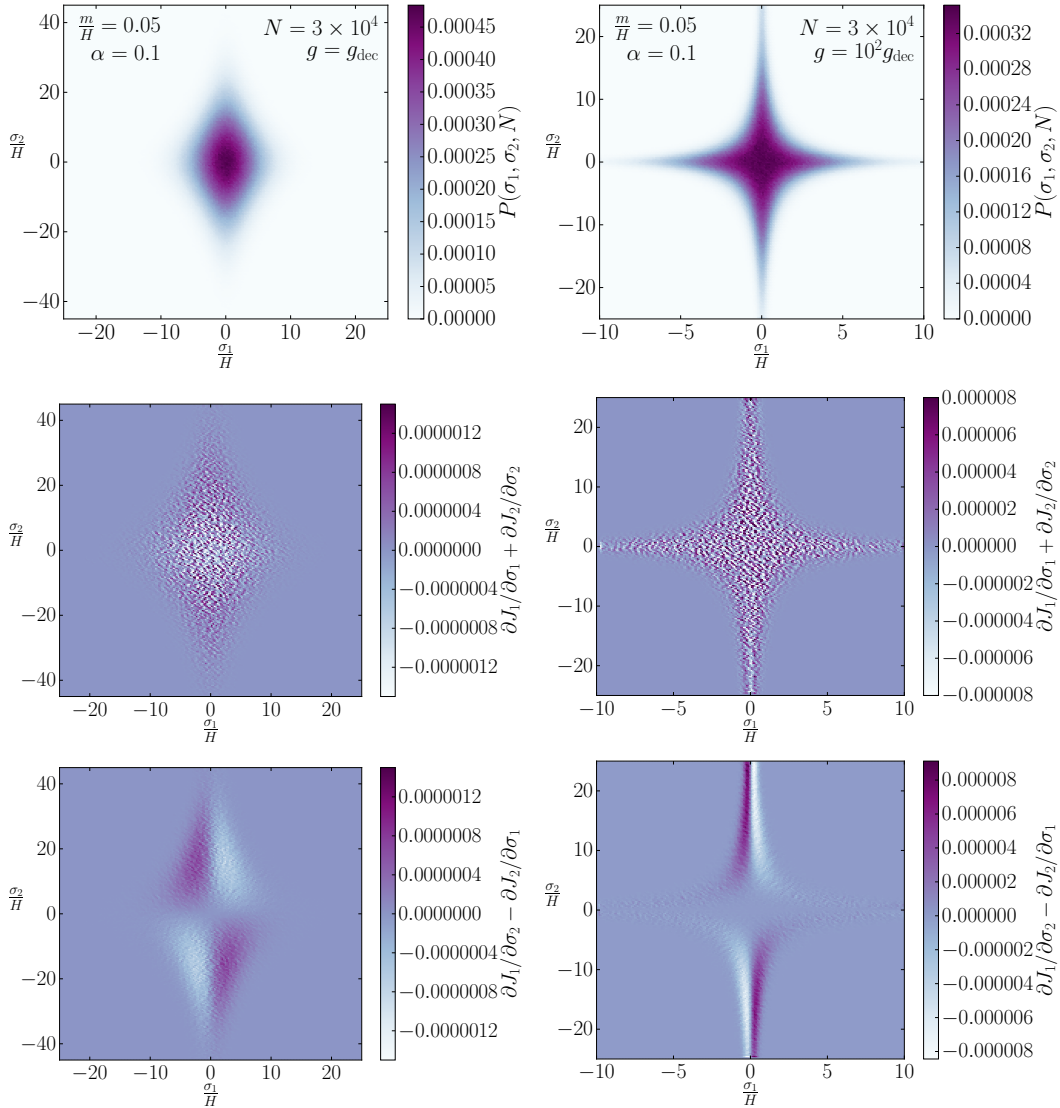


Figure 10. Using specific parameter choices of the V_B potential (see Eq. (3.9)) we plot the binned stationary probability density P_{stat} (top row), probability current divergence $\nabla \cdot \mathbf{J}$ (middle row) and the only non-zero component of the probability current curl $\nabla \times \mathbf{J}$ (bottom row). These have all been numerically obtained from 10^7 realisations of Eq. (1.1) in the `nfield` code.

In Fig. 9 and Fig. 10 we have plotted some binned realisations of Eq. (1.1) that are used in the code. These plots can also serve as a useful tool to test for numerical convergence, e.g. to check that no arbitrary asymmetry has appeared or if the divergence of the probability current has not vanished due to elevated numerical noise. In such instances, the code may simply be rerun with more realisations to ensure convergence. Even though 10^7 realisations were used for these plots, numerical noise (and noise from a finite number of samples) still appears for those values of $\nabla \cdot \mathbf{J}$ and $\nabla \times \mathbf{J}$ which are meant to vanish. Up to this noise amplitude, however, a strong signal can still be seen in $\nabla \times \mathbf{J}$ for the $g = 10^2 g_{\text{dec}}$ potential in Fig. 10, and we leave further improvements to these visualisations for future work.

References

- [1] A. A. Starobinsky and J. Yokoyama, *Equilibrium state of a selfinteracting scalar field in the De Sitter background*, *Phys. Rev.* **D50** (1994) 6357–6368, [[astro-ph/9407016](#)].
- [2] A. D. Linde and V. F. Mukhanov, *Nongaussian isocurvature perturbations from inflation*, *Phys.Rev.* **D56** (1997) 535–539, [[astro-ph/9610219](#)].
- [3] K. Enqvist and M. S. Sloth, *Adiabatic CMB perturbations in pre - big bang string cosmology*, *Nucl.Phys.* **B626** (2002) 395–409, [[hep-ph/0109214](#)].
- [4] D. H. Lyth and D. Wands, *Generating the curvature perturbation without an inflaton*, *Phys.Lett.* **B524** (2002) 5–14, [[hep-ph/0110002](#)].
- [5] T. Moroi and T. Takahashi, *Effects of cosmological moduli fields on cosmic microwave background*, *Phys.Lett.* **B522** (2001) 215–221, [[hep-ph/0110096](#)].
- [6] N. Bartolo and A. R. Liddle, *The Simplest curvaton model*, *Phys.Rev.* **D65** (2002) 121301, [[astro-ph/0203076](#)].
- [7] K. Enqvist, R. N. Lerner, O. Taanila and A. Tranberg, *Spectator field dynamics in de Sitter and curvaton initial conditions*, *JCAP* **1210** (2012) 052, [[1205.5446](#)].
- [8] R. J. Hardwick, V. Vennin, C. T. Byrnes, J. Torrado and D. Wands, *The stochastic spectator*, [1701.06473](#).
- [9] R. J. Hardwick, V. Vennin and D. Wands, *A Quantum Window Onto Early Inflation*, [1705.05746](#).
- [10] A. Heidmann, R. J. Horowicz, S. Reynaud, E. Giacobino, C. Fabre and G. Camy, *Observation of quantum noise reduction on twin laser beams*, *Phys. Rev. Lett.* **59** (Nov, 1987) 2555–2557.
- [11] L. Grishchuk, H. A. Haus and K. Bergman, *Generation of squeezed radiation from vacuum in the cosmos and the laboratory*, *Phys. Rev. D* **46** (Aug, 1992) 1440–1449.
- [12] L. P. Grishchuk and Y. V. Sidorov, *Squeezed quantum states of relic gravitons and primordial density fluctuations*, *Phys. Rev. D* **42** (Nov, 1990) 3413–3421.
- [13] R. J. Hardwick, T. Markkanen, S. Nurmi and V. Vennin, *Article in preparation.*, [XXXX.XXXXX](#).
- [14] J. Grain and V. Vennin, *Stochastic inflation in phase space: Is slow roll a stochastic attractor?*, *JCAP* **1705** (2017) 045, [[1703.00447](#)].
- [15] N. C. Tsamis and R. P. Woodard, *Stochastic quantum gravitational inflation*, *Nucl. Phys.* **B724** (2005) 295–328, [[gr-qc/0505115](#)].
- [16] T. S. Bunch and P. C. W. Davies, *Quantum Field Theory in de Sitter Space: Renormalization by Point Splitting*, *Proc. Roy. Soc. Lond.* **A360** (1978) 117–134.
- [17] N. D. Birrell and P. C. W. Davies, *Quantum Fields in Curved Space*. Cambridge Monographs on Mathematical Physics. Cambridge Univ. Press, Cambridge, UK, 1984, [10.1017/CBO9780511622632](#).
- [18] T. Markkanen and A. Rajantie, *Massive scalar field evolution in de Sitter*, *JHEP* **01** (2017) 133, [[1607.00334](#)].
- [19] C. P. Burgess, R. Holman, L. Leblond and S. Shandera, *Breakdown of Semiclassical Methods in de Sitter Space*, *JCAP* **1010** (2010) 017, [[1005.3551](#)].
- [20] R. P. Woodard, *Cosmology is not a Renormalization Group Flow*, *Phys. Rev. Lett.* **101** (2008) 081301, [[0805.3089](#)].
- [21] J. Tokuda and T. Tanaka, *Statistical nature of infrared dynamics on de Sitter background*, [1708.01734](#).

- [22] A. A. Starobinsky, *Dynamics of Phase Transition in the New Inflationary Universe Scenario and Generation of Perturbations*, *Phys. Lett.* **117B** (1982) 175–178.
- [23] A. A. Starobinsky, *Multicomponent de Sitter (Inflationary) Stages and the Generation of Perturbations*, *JETP Lett.* **42** (1985) 152–155.
- [24] H. Risken, *The Fokker-Planck Equation, Springer Series in Synergetics* **18** (1989) .
- [25] H. Assadullahi, H. Firouzjahi, M. Noorbala, V. Vennin and D. Wands, *Multiple Fields in Stochastic Inflation*, *JCAP* **1606** (2016) 043, [[1604.04502](#)].
- [26] Y. Ema, M. Karciauskas, O. Lebedev, S. Rusak and M. Zatta, *Higgs-Inflaton Mixing and Vacuum Stability*, [1711.10554](#).
- [27] A. Ashoorioon, H. Firouzjahi and M. M. Sheikh-Jabbari, *M-flation: Inflation From Matrix Valued Scalar Fields*, *JCAP* **0906** (2009) 018, [[0903.1481](#)].
- [28] M. Fairbairn, T. Markkanen and D. Rodriguez-Roman, *Horizon Feedback Inflation*, [1712.07977](#).
- [29] D. Glavan, T. Prokopec and A. A. Starobinsky, *Stochastic dark energy from inflationary quantum fluctuations*, [1710.07824](#).
- [30] K. Enqvist, R. J. Hardwick, T. Tenkanen, V. Vennin and D. Wands, *A novel way to determine the scale of inflation*, [1711.07344](#).
- [31] K. Freese, E. I. Sfakianakis, P. Stengel and L. Visinelli, *The Higgs Boson can delay Reheating after Inflation*, [1712.03791](#).
- [32] A. J. Roberts, *Modify the Improved Euler scheme to integrate stochastic differential equations*, *ArXiv e-prints* (Oct., 2012) , [[1210.0933](#)].